Title

A metabolite specific 3D stack-of-spirals bSSFP sequence for improved bicarbonate imaging in hyperpolarized [1-13C]Pyruvate MRI

Authors

Liu, Xiaoxi
Tang, Shuyu
Cui, Di
et al.

Publication Date

2023-08-01

DOI

10.1016/j.jmr.2023.107518

Peer reviewed

HHS Public Access

Author manuscript

J Magn Reson. Author manuscript; available in PMC 2024 August 01.

Published in final edited form as:

J Magn Reson. 2023 August ; 353: 107518. doi:10.1016/j.jmr.2023.107518.

A Metabolite Specific 3D Stack-of-Spirals bSSFP Sequence for Improved Bicarbonate Imaging in Hyperpolarized [1-^{13}C]Pyruvate MRI

Xiaoxi Liu[1], **Shuyu Tang**[2], **Di Cui**[1], **Robert A. Bok**[1], **Hsin-Yu Chen**[1], **Jeremy W. Gordon**[1], **Zhen J. Wang**[1], **Peder E.Z. Larson**[1,3,*]

[1]Department of Radiology and Biomedical Imaging, University of California, San Francisco, San Francisco, CA, USA

[2]Vista.ai Inc., Los Altos, CA, USA

[3]Graduate Program in Bioengineering, University of California, Berkeley and San Francisco, San Francisco, CA, USA

Abstract

^{13}C-bicarbonate is a crucial measure of pyruvate oxidation and TCA cycle flux, but is challenging to measure due to its relatively low concentration and thus will greatly benefit from improved signal-to-noise ratio (SNR). To address this, we developed and investigated the feasibility of a 3D stack-of-spirals metabolite-specific balanced steady-state free precession (MS-bSSFP) sequence for improving the SNR and spatial resolution of dynamic ^{13}C-bicarbonate imaging in hyperpolarized [1-^{13}C]pyruvate studies. The bicarbonate MS-bSSFP sequence was evaluated by simulations, phantoms studies, preclinical studies on five rats, brain studies on two healthy volunteers and renal study on one renal cell carcinoma patient. The simulations and phantom results showed that the bicarbonate-specific pulse had minimal perturbation of other metabolites (<1%). In the animal studies, the MS-bSSFP sequence provided an approximately 2.6–3 × improvement in ^{13}C-bicarbonate SNR compared to a metabolite-specific gradient echo (MS-GRE) sequence without altering the bicarbonate or pyruvate kinetics, and the shorter spiral readout in the MS-bSSFP approach reduced blurring. Using the SNR ratio between MS-bSSFP and MS-GRE, the T_2 values of bicarbonate and lactate in the rat kidneys were estimated as 0.5 s and 1.1 s, respectively. The in-vivo feasibility of bicarbonate MS-bSSFP sequence was demonstrated in two human brain studies and one renal study. These studies demonstrate the potential of the sequence for in-vivo applications, laying the foundation for future studies to observe this relatively low concentration metabolite with high-quality images and improve measurements of pyruvate oxidation.

Keywords

Hyperpolarized ^{13}C; bSSFP; metabolic imaging; ^{13}C-bicarbonate; SNR; pyruvate oxidation

[*]Corresponding Author: Peder E.Z. Larson, 1700 4th St, Byers Hall Room 102C, San Francisco, CA, USA 94143, peder.larson@ucsf.edu.

1. Introduction

Hyperpolarized (HP) magnetic resonance imaging (MRI) is a powerful non-invasive modality for investigating in-vivo metabolic pathways, including tumor characterization, treatment selection, and treatment response monitoring.[1–3] After hyperpolarization by dynamic nuclear polarization (DNP) technique, the transient signal of HP ^{13}C-labelled components can increase by more than ten-thousand fold over its signal at thermal equilibrium.[4] However, HP signal of ^{13}C-labelled compounds decay quickly back to the thermal equilibrium state once leaving the polarizer, which is characterized by T_1 (~30 s).

MRI with HP [1-^{13}C]pyruvate, the most commonly used HP agent, can provide real-time in vivo cellular energy metabolism, including kinetic reactions and enzyme activities, and has been used in numerous human studies.[5–11] In cells, [1-^{13}C]pyruvate can be converted to lactate by lactate dehydrogenase (LDH) or converted to acetyl coenzyme A and carbon dioxide (CO_2) by pyruvate dehydrogenase (PDH).[12,13] LDH enzymatically mediates the pyruvate to lactate conversation in glycolysis, and [1-^{13}C]lactate has been suggested as a biomarker correlating with LDH activity.[13–15] At the same time, PDH controls pyruvate flux into mitochondria to feed the tricarboxylic acid (TCA) cycle. Since the downstream product CO_2 is rapidly equilibrated with bicarbonate, ^{13}C-bicarbonate is a surrogate marker for PDH activity.[16,17] In previous HP studies, pyruvate-to-lactate conversion has been successfully used in detecting abnormal metabolism in cancer.[5,6,18–20] Imaging of pyruvate-to-bicarbonate conversion is also desirable, where changes in bicarbonate are potential biomarkers of heart disease[19,21], brain tumors[22], liver[23], and kidney diseases[24]. However, bicarbonate has a lower concentration than lactate, which makes bicarbonate measurements more challenging. Therefore, improving the SNR of ^{13}C-bicarbonate would greatly improve the capabilities of HP [1-^{13}C]pyruvate studies.

Due to the irreversible and rapid decay of the HP [1-^{13}C]pyruvate magnetization, which limits both temporal and spatial SNR, several advanced methods have been developed to improve the SNR of measured HP ^{13}C-labelled metabolites. In the acquisition, optimized quality control steps can reduce the time-to-injection[25]; multichannel receiver coils can provide improved SNR over large volumes[26]; fast imaging methods[27–29] with variable resolution acquisition[30] can improve SNR for the measured metabolites with low concentration; and dynamic, metabolite-specific flip angles can improve SNR[31,32]. Refocused imaging methods such as multi spin echo (SE)[33–36] and balanced steady-state free precession[28,29,37,38] sequences have also demonstrated SNR improvements over gradient echo sequences by repeated sampling of the transverse magnetization.

In this work, we developed and assessed a bicarbonate-specific acquisition method to provide SNR improvements and higher spatial resolution of bicarbonate data in vivo. In previous studies, metabolite-specific balanced steady-state free precession (MS-bSSFP) sequences[28,29,37,38] have been proven to create at least 2-fold SNR improvements in ^{13}C-lactate[29] imaging and ^{13}C-urea[38] imaging. MS-bSSFP uses lower flip angles compared to SE sequences, avoiding potential saturation of the hyperpolarized magnetization that can be severe, e.g. due to imperfect refocusing pulse profile at the edges of slice or RF coil[40]. As ^{13}C-bicarbonate has intrinsically lower concentrations compared to ^{13}C-lactate

and ^{13}C-urea, the sequence design is more challenging. To address this issue, we designed the sequence with a more selective RF pulse, including reduced ripples, to reduce undesired excitation of other metabolites in the frequency profile. Furthermore, as bSSFP images are T_2/T_1-weighted, the in vivo T_2 is encoded in the signal and thus can be estimated from this data. The designed MS-bSSFP sequence for ^{13}C-bicarbonate was tested in simulation, validated and characterized in thermal phantoms and rat models, and applied in human studies demonstrating feasibility in the brain and kidneys.

2. Methods

Sequence Design

The proposed bicarbonate MS-bSSFP sequence is shown in Figure S1(a), which used same structure as our previous work[29,38]. The design of a bicarbonate-specific RF pulse was based on a multiband RF pulse model to minimize the duration of the pulse (4.2 ms).[29,41,42] Considering the B_0 inhomogeneity in the target regions is always in a limited range (Figure 4 and Figure S9), a 40 Hz passband was designed on bicarbonate frequency, and 40 Hz stopband was designed on other metabolite frequencies: with 0.2% ripples on pyruvate frequency (322 Hz) and pyruvate hydrate frequency (589 Hz), and with 0.8% ripples on alanine frequency (507 Hz) and lactate frequency (717 Hz) (Figure 1(a)).

One of the primary limitations of bSSFP sequences is that the steady state magnetization varies as a function of off-resonance frequencies, determined by the TR. However, the minimum TR is limited by the duration of spectrally-selective RF pulse and the readout time required to obtain adequate spatial resolution. The optimal TR in this sequence was set as 9.8 ms to achieve reasonable spatial resolution and maximize the frequency differences from banding artifact locations to other metabolites (pyruvate, lactate, alanine, pyruvate-hydrate) resonance frequencies.

To compare the proposed bicarbonate MS-bSSFP sequence and conventional 2D metabolite-specific gradient echo (MS-GRE) sequence, the flip angle of bSSFP was set as 60°, which is approximately equivalent to an optimized a GRE flip angle of 30° that we commonly use for HP studies[43], shown in Figure S2(a). This 3D bicarbonate MS-bSSFP sequence was implemented on a 3 T GE clinical MRI scanner (MR750, GE Healthcare, Waukesha, WI) controlled by RTHawk software (Vista.ai, Los Altos, CA) for hyperpolarized ^{13}C acquisition.

Simulations

The RF pulse and sequence excitation profiles were calculated using Bloch simulation, shown in Figure 1. In the preparation TRs, 6 catalyzation pulses with increasing flip angles of 3°, 7.2°, 22.8°, 41.4°, 55.8°, 60° were used. In the imaging TRs, the parameters included flip angle = 60°, number of excitations = 64, T_1 = 25 s, T_2 = 1 s, and TR = 9.8 ms. The mean of transverse magnetization in all imaging TRs were calculated as excitation profile of bSSFP acquisition.

Considering the difference between T_1-weighted GRE data and T_2/T_1-weighted bSSFP data, the dynamic signal ratio of GRE and bSSFP in bicarbonate and lactate acquisition were

simulated using analytic models[44,45] to compare the SNR and relaxation effects expected in HP data. The simulation parameters included T_1 = 25 s, T_2* = 35 ms, temporal resolution = 3 s, flip angle = 30°/60° (GRE/bSSFP), readout duration = 25/3.8 ms (GRE/bSSFP). In the bSSFP sequence, TR = 9.8/15.3 ms (bicarbonate/lactate), and the echo train length for each time point = 64.

To evaluate MS-bSSFP sequence and MS-GRE sequence, the point spread functions were simulated with parameters: T_2* = 35/70 ms,[46] readout duration = 25/3.8 ms (GRE/bSSFP), off-resonance frequency = 0/10/20 Hz. All signals were normalized by the maximum signal without off-resonance effect and T_2* relaxation.

Phantom Experiment

The phantom experiments were performed to measure the excitation profile of the designed RF pulse and bSSFP sequence. One ^{13}C-enriched 8 M urea phantom doped with a Gd-based contrast agent ($T_1 \approx$ s) was scanned by the 3 T GE scanner with a ^{13}C transceiver animal birdcage coil (1-channel). To measure the excitation profile at all metabolite frequencies, the off-resonance frequencies of ^{13}C signal were set with ±40 Hz frequency ranges of pyruvate, pyruvate hydrate, alanine, lactate and bicarbonate, respectively. Other parameters included size of phantom (diameter 1cm and length 6.5 cm), resolution = 1×1 cm^2, TR = 500 ms, flip angle = 60°, and NEX = 400.

Animal Experiment

Animal studies of hyperpolarized [1-^{13}C]pyruvate imaging were conducted on five healthy adult Sprague-Dawley (SD) rats with three identical injections to quantify the 3D ^{13}C-bicarbonate MS-bSSFP sequence in vivo using hyperpolarized [1-^{13}C]pyruvate. All animal experiments were approved by the University of California, San Francisco Institutional Animal Care and Use Committee (IACUC). The rats were anesthetized and cannulated in the lateral tail vein.[38]

The hyperpolarized solution containing 60 uL [1-^{13}C]pyruvate acid, 15 mM OX063 trityl radical, and 1.5 mM Gd-DOTA was polarized using microwaves in a SPINlab system for about 4 hours. The polarized sample was then quickly dissolved in sterile water and neutralized with a buffer solution. In each scan, a 2.5 mL dosage of hyperpolarized solution injected into the rat via the tail vein over a period of 12 seconds.

Animal data were acquired on a 3 T GE clinical scanner with a ^{1}H/^{13}C transceiver animal birdcage coil (1-channel). Table 1(a) shows the sequence parameters of hyperpolarized [1-^{13}C]pyruvate animal studies.

Considering the concentrations of three metabolites are quite different, a variable resolution approach was used to provide balanced signal amplitudes.[30] The 2D MS-GRE sequence consists of a spectral-spatial excitation pulse[47] (80 Hz passband, 770 Hz stopband, 25.17 ms duration) and a single-shot spiral readout (25 ms duration). The imaging sequences were automatically triggered after the end of injection and included real-time frequency calibration.[48] In Experiment A, a real-time B_1^+ calibration[49] was performed after frequency calibration. In Experiment B and C, only B_1^+ maps were measured but the B_1 scaling

was kept same as the value in Experiment A for consistency in comparisons. Before and after hyperpolarized ^{13}C imaging, anatomical localizers were acquired by a proton bSSFP sequence (FOV 16×16×12 cm^3, resolution 1×1×2 mm^3). In addition, the B_0 field map was acquired by a proton IDEAL IQ sequence (FOV 20×20 cm^2, resolution 1.25×1.25×10 mm^3) with local shimming. The shimming values were also used during ^{13}C data acquisition.

Human Studies

To demonstrate and evaluate the feasibility of 3D bicarbonate MS-bSSFP strategy in the clinical setting, brain studies were performed on two healthy volunteers and one renal study was performed on a renal carcinoma cell (RCC) patient. All human studies were performed under UCSF institutional review board approved protocols.

The contrast agents used for imaging, containing 1.47 g Good Manufacturing Practices (GMP) [1-^{13}C]pyruvate acid and 15 mM electron paramagnetic agent AH111501, were polarized in a 5 T SPINlab polarizer for 3–4 hours before being rapidly dissolved, filtered and neutralized. Prior to injection, the hyperpolarized probe was passed through a 0.2 μm sterile filter that was integrity tested. Finally, a 0.43 mL/kg body weight dosage of hyperpolarized [1-^{13}C]pyruvate followed by a 20 mL saline flush was injected at 5 mL/s.

For the brain studies, each of two healthy volunteers received a single hyperpolarized [1-^{13}C]pyruvate injection. The first study (Male, Age 59) was performed during our initial testing of the regional bolus tracking and real-time B_1^+ calibration methods[49], and for comparisons we matched study parameters as close as possible for the second study (Male, Age 41) that used the ^{13}C-bicarbonate MS-bSSFP acquisition. This design was chosen to test the method with limited availability at the time of SPINlab fluid paths for human studies. For both studies, $^1H/^{13}C$ imaging data from the human brain were acquired using a birdcage coil for RF transmit with an integrated 24-channel receiver (Rapid Biomedical, Würzburg, Germany). Table 1(b) shows the parameters for the ^{13}C human brain data acquisition. In particular, we matched the voxel size, temporal resolution, and GRE flip angles, as these have the most significant impact on the resulting dynamic signal levels. Hyperpolarized ^{13}C data acquisition started 5 s after the saline flush finished. In each scan, one real-time frequency calibration was performed over a central axial slice of the brain to measure the [1-^{13}C]pyruvate frequency. The spectrum is shown in Figure S8. Multi-slice Bloch-Siegert B_1^+ maps were acquired as a reference and the transmit gain was calibrated by the middle slice B_1^+ scale within the brain. Similar to the Experiment A and B in animal studies, the data of [1-^{13}C]pyruvate and [1-^{13}C]lactate were collected by 2D MS-GRE sequences and ^{13}C-bicarbonate data were acquired by the 3D MS-bSSFP sequence and 2D MS-GRE sequence in separate experiments.

For the renal study, one 61-year-old female patient with a multilobulated solid and cystic mass on the left kidney participating in a kidney cancer trial was recruited to demonstrate the feasibility of 3D bicarbonate MS-bSSFP. ^{13}C were acquired using a semi-flexible transmitter and 8-channel receive array (QTAR system, Clinical MR Solutions, Brookfield WI, USA). Table 1(c) shows the acquisition setting and parameters in ^{13}C renal study. The other acquisition settings were the same as previous studies[5]. Note that only the unaffected kidney

of this subject is shown because the imaging results in the kidney with the renal mass were inconclusive.

For brain studies, proton anatomical images were acquired with a 3D T_1-weighted Brain Volume imaging (BRAVO) sequence with an FOV of 25.6×25.6×19.6 cm^3 and a resolution of 1×1×0.5 mm^3. For renal study, proton anatomical images were acquired with a single-shot fast spin echo (FSE) sequence with an FOV of 42×42 cm^2 and a resolution of 1.6×1.6 mm^2, slice thickness 6 mm. Additionally, the B_0 field maps were measured using an IDEAL IQ sequence (Brain study: FOV 34×34 cm^2, resolution 1.33×1.33×3 mm^3, 20 slices; Renal study: FOV 44×44 cm^2, resolution 1.72×1.72×10 mm^3, 16 slices) and localized gradient linear shimming of the targeted organ volume to improve the B_0 field homogeneity prior to the hyperpolarized ^{13}C MR acquisition.

Image Reconstruction and Data Analysis

For both animal and human studies, data processing was utilized Matlab 2021 software (Mathworks Inc.). The spiral data were processed by gridding[50] (http://web.stanford.edu/class/ee369c/mfiles/gridkb.m) and inverse Fourier transformation. In the human study, multi-channel data were processed by pre-whitening[50] and coil combination[51] using coil sensitivity maps estimated from the pyruvate data. The normalization for each metabolite's hyperpolarized ^{13}C data were performed using the standard deviation of the noise-only data acquired at the last time point. The metabolite area-under-curve (AUC) SNR ratio images were calculated by the division between two metabolite AUC images with noise normalization. The dynamic hyperpolarized ^{13}C signals of all metabolites were additionally normalized according to the maximum signal of [1-^{13}C]pyruvate.

In the animal studies, to estimate the in vivo T_2 of bicarbonate and lactate, a dynamic SNR ratio between 3D MS-bSSFP data and 2D MS-GRE data were measured on the kidney of each rat (N = 5) over 15 time points including a noise offset correction by power analysis method[52]. To correlate the metabolite hyperpolarized data across two injections, normalization factors were calculated by the maximum pyruvate signal in each experiment. Approximate estimates of the in vivo T_2 values were based on visual inspection and matching of the simulated and experimental dynamic SNR ratio curves.

In the human brain study, a region-of-interest (ROI) placed on the whole brain in the brain was drawn to measure the dynamic data of all metabolite signals. For display reasons, the bicarbonate dynamic images were displayed with the urea phantom region masked out.

3. Results

Simulations and Phantom Studies

The Bloch equation was used to simulate the excitation profiles of 3D bicarbonate MS-bSSFP sequence. Figure 1(b) shows the average transverse magnetization over all readouts by Bloch simulation, and the green dashed lines showed banding artifacts occurring over 30 Hz away from the other metabolites resonance frequencies. When a 60° excitation was simulated, a frequency shift of ±20 Hz led to a 20% increase in signal intensity for on-resonance bicarbonate. In the ±35 Hz frequency shift range around the other

metabolites frequencies, the simulated excited signal is always lower than 1% of bicarbonate on-resonance frequency signal.

The urea thermal phantom study, presented in Figure 1(d), was used to validate the excitation profiles of 3D bicarbonate MS-bSSFP sequence. The measured excitation profile matched well with the simulation results. Simulations of the off-resonance point spread function (Figure S3) show that there will be significant blurring artifacts if there is excitation of undesired metabolites.

To compare the signal response and choice of flip angle between MS-bSSFP and MS-GRE sequences, the AUC magnetizations were simulated for analysis (Figure S2). In the MS-GRE sequence, both T_1 and flip angle affect the AUC magnetization, with the highest value being achieved at a 30° flip angle for the chosen TR. Meanwhile, in the MS-bSSFP sequence, the AUC magnetization depends on T_2, T_1 and flip angle. Here, we assumed that the T_1 is the same for each metabolite. The optimal flip angle of the MS-bSSFP sequence becomes higher with an increase in T_2, as presented in Figure S2(b). However, both [1-^{13}C]pyruvate and [1-^{13}C]lactate have measured $T_2 < 1$ s[36,53] so we expect ^{13}C-bicarbonate to be similar. Based on this we expect the optimal flip angle for the bicarbonate 3D MS-bSSFP sequence is around 40°−60°.

Evaluating the point spread functions of the single-shot spiral MS-GRE sequence and 4-interleave stack-of-spirals used in the MS-bSSFP sequence, Figure 6 shows that the MS-GRE trajectory will suffer more from off-resonance artifacts and T_2* blurring than the MS-bSSFP trajectory. These simulations also indicate that off-resonance artifacts are much more significant over the ranges of off-resonance (10 an 20 Hz) and T_2* (35 and 70 ms) selected.

Animal Studies

Comparisons of 3D MS-bSSFP and 2D MS-GRE sequences analyzed in the rat's kidney and cardiac slices are shown in Figure 2. In the animal studies, [1-^{13}C]pyruvate imaging results were compared using two different acquisition methods with three injections (Figure 2). Comparing bicarbonate AUC images in Experiment A&C and B, the banding artifacts are not observed on the 3D MS-bSSFP images. This was consistent with the B_0 map which shows the on-resonance frequencies of the heart and kidney that fell in the frequency range of the passband ($\Delta B_0 < \frac{1}{TR} = \pm 51$ Hz). In the comparison of lactate AUC images and bicarbonate AUC images between Experiment B and Experiment C, the right kidney and heart shows more blurring artifact with the lactate and bicarbonate 2D MS-GRE sequences compared to the 3D MS-bSSFP sequence. This can be ascribed to the larger off-resonance frequency with the field map showing −17 Hz at right kidney and −32 Hz at the edge between heart and lungs, as expected from the simulation of the point spread function in Figure 6. The SNR ratio maps show that the 3D MS-bSSFP sequence leads to improved SNR when compared to the 2D MS-GRE sequence for both lactate and bicarbonate. In both the heart and kidneys, the 3D MS-bSSFP bicarbonate sequence shows a mean±standard deviation of 3.02±0.93× and 2.58±0.54× SNR improvement over the 2D MS-GRE bicarbonate sequence (Figure 2).

Bicarbonate and lactate SNR ratios between 3D MS-bSSFP data and 2D MS-GRE data over the renal regions of 5 healthy Sprague Dawley rats are presented in Figure 3(a&b). Comparing to 2D MS-GRE sequences, the 3D MS-bSSFP bicarbonate sequence shows an approximately 2.7× SNR increasement in the first five time points which decreases in the later time points. The renal dynamic SNR ratio of bicarbonate data approximately matches the T_2 = 0.5 s curve in the simulation results (Figure 3(c)). Similarly, comparing the lactate signal ratio of 3D MS-bSSFP and 2D MS-GRE in the simulation (Figure 3(d)) and rat kidney results (Figure 3(b)), the data approximately matches the simulated T_2 = 1.1 s curve.[24]

The comparison of dynamic HP ^{13}C kidney images acquired by the 3D MS-bSSFP and 2D MS-GRE sequences are presented in Figure S4. The off-resonance blurring artifacts in 2D MS-GRE data are clearly shown in both lactate images and bicarbonate images, which is consistent with the simulation of point spread function at off-resonance frequencies (in Figure 6). Due to the short T_2* (~65 ms)[45] and intrinsic lower concentration[22] of bicarbonate, bicarbonate data were acquired with lower resolution to obtain sufficient SNR.[30] Therefore, bicarbonate images suffer from larger partial volume effect than lactate images, and meanwhile, the short T_2* also leads to severe blurring artifact in 2D MS-GRE images.

The dynamic curves of pyruvate, lactate, and bicarbonate signals in one animal study are shown in Figure S5. All signals have been normalized by the first timepoint pyruvate signal of each injection and corresponding noise signals. A larger signal fluctuation was observed in the heart slice due to the higher signal level and heart motion. The signal decay rate of both lactate and bicarbonate acquired by bSSFP sequence were found to be similar to that of pyruvate acquired by 2D MS-GRE sequence.

Human Studies

In the HP [1-^{13}C]pyruvate imaging human brain study, we compared 3D MS-bSSFP and 2D MS-GRE sequences on two healthy adult volunteers (Figure 4 and Figure S7) with pyruvate, lactate, bicarbonate, and bicarbonate-to-lactate SNR ratio AUC images. Similar to the animal experiments, no banding artifacts were observed in 3D MS-bSSFP bicarbonate images. The 24-channel head coil produced a B_1^+ field that was largely between 90–110% of the desired value (Figure S6), which will lead to approximately ±10% variation in metabolite amplitudes across the brain. Comparing the bicarbonate-to-lactate SNR ratio AUC images between these two studies in healthy volunteers, higher values are found across the brain for the 3D MS-bSSFP sequence indicating it provides a higher SNR than the 2D MS-GRE sequence.

Comparing the dynamic signal curve of bicarbonate in Subject A and Subject B (Figure 4), a 1.86× higher SNR was measured across the whole brain for 3D MS-bSSFP compared to 2D MS-GRE for bicarbonate. The distribution of bicarbonate primarily in the gray matter is also more clearly visualized in the dynamic 3D MS-bSSFP images.

In the human renal study, the 3D MS-bSSFP sequence was demonstrated to successfully acquire lactate and bicarbonate data in the abdomen, shown in Figure 5. The abdomen

typically has a larger B_0 field inhomogeneity compared to the head (Figure S9), but we did not observe any artifacts or distortion. The lactate and bicarbonate images show excellent signal localized to the kidney. Both lactate-to-pyruvate ratio map and bicarbonate-to-pyruvate ratio map show a consistent intensity pattern over the cortex of the kidney.

4. Discussion

In this study, we developed and investigated a 3D MS-bSSFP sequence for ^{13}C-bicarbonate imaging follow HP [1-^{13}C]pyruvate injection with a center-out spiral readout and demonstrated that it provides higher SNR than conventional 2D MS-GRE sequence and has the potential to improve the spatial resolution. The excitation profile of bicarbonate-specific excitation pulse was validated by the urea phantom experiments and the 3D MS-bSSFP sequence was demonstrated by pre-clinical studies with no banding artifacts. The bicarbonate data showed improvements of around 2.6±0.5× and 3±0.9× in SNR for 3D MS-bSSFP compared to 2D MS-GRE on the kidneys and heart in healthy Sprague Dawley rats. In the human brain studies, the 3D MS-bSSFP bicarbonate sequence was compared with 2D MS-GRE bicarbonate sequence and showed a 1.86× SNR improvement. The human renal study demonstrated the feasibility of 3D MS-bSSFP bicarbonate sequence in the abdomen as well where, compared to the head, a larger FOV and different RF coils are required and there are notable differences in spatial distribution and perfusion. In particular, there is the potential for larger variations in B_0 (Figure S9) but these did not distort the resulting images.

Compared to GRE sequences, bSSFP sequences can efficiently use magnetization via refocusing the spins by a set of balanced gradients, instead of spoiling the residual magnetization after each readout. This allows for larger flip angles to be used in MS-bSSFP compared to MS-GRE and provides higher SNR. Comparing the signal decay curve between 3D MS-bSSFP bicarbonate/lactate and 2D MS-GRE pyruvate in Figure S5, they show similar signal decay rates, indicating the magnetization is well-preserved for dynamic imaging. With a more efficient magnetization excitation, 3D MS-bSSFP sequence is more suitable for HP ^{13}C-bicarbonate imaging than 2D MS-GRE sequence. Compared to SE sequences, bSSFP sequences eliminate the need to apply 180° pulses to refocus the magnetization, which are challenging to use in dynamic HP metabolic imaging because variations in refocusing pulse flip angles, for example in regions at the edge of RF transmit coils due to B_1^+ inhomogeneity or at the slice transition regions, can lead to rapid depolarization. Both SE and bSSFP signal have T_2 encoding, which could be valuable for quantification of T_2 values that have a big impact on the acquisition. Both sequences require a long time to create measurable T_2 differences due to the relatively long T_2 of ^{13}C-labelled metabolites present[39]. Because T_2 effect can be restored in longitudinal magnetization and stack in later time points, the T_2 can be estimated by combining different timepoint dynamic signals for fitting as shown in these results (Figure 3). The MS-bSSFP technique requires 3D encoding, since the RF pulses are only spectrally-selective, and we also rely on the spatial selectivity from the RF transmit coil.

Both spiral and Cartesian EPI trajectories are well-suited for bSSFP technique in hyperpolarized substrates because of the high duty cycle and efficient trajectories.[27–29]

However, considering the limited TR, multiple interleaves are also required when applying spiral or EPI trajectories in bSSFP sequences. With the benefit of a shorter TE than the EPI readout, the spiral readout can improve the SNR for ^{13}C metabolites with a shorter T_2*, while an EPI trajectory is more sensitive to motion effects and the T_2* difference between metabolites has the potential to affect quantification. Therefore, a center-out spiral readout was utilized in the sequence for better SNR and motion robustness. The downsides of the spiral trajectory are that it is more sensitive to gradient fidelity and suffers from strong off resonance blurring artifacts. More severe blurring artifacts can furtherly reduce the signal intensity (Figure 6). In the design of 3D MS-bSSFP bicarbonate sequence, we used an interleaved spiral readout to shorten the readout duration for reducing off-resonance effects and to achieve the optimal TR for bSSFP sequence.

The bicarbonate MS-bSSFP required 627 ms for acquiring the 64 readouts for encoding the 3D volume, over which changes in signal amplitude due to relaxation or metabolic conversion as well as motion could lead to blurring and artifacts. However, based on prior HP studies we expect the changes in ^{13}C-bicarbonate signal and motion of the kidneys and brain to be relatively small over this duration. We also did not observe any apparent artifacts. Translating this approach into cardiac metabolic imaging maybe challenging due to heart motion, although maybe addressable by shortening the 3D acquisition through acceleration methods such as parallel imaging and/or compressed sensing.

Due to a recent shortage of available SPINlab fluid paths for human studies, we compared results between single injections on two different healthy volunteers. The volunteers were both males, aged 41 and 59. Prior work has shown that the lactate and bicarbonate distribution, measured as a topography, was preserved across healthy subjects (N=14, aged 23–77)[54]. Another study of four healthy volunteers measured bicarbonate:pyruvate ratios of 0.07 ± 0.04 across the brain.[55] This amount of variation is less that the ~2-fold signal improvement we observed for MS-bSSFP versus GRE comparing across our two subjects. Furthermore, the improvement in bicarbonate image quality was clear for the same voxel sizes, and our animal studies had consistent improvements in bicarbonate signal with MS-bSSFP. Taken together, we believe that the bicarbonate MS-bSSFP method was providing improved SNR in the human brain, which agrees with the results in the rat studies.

Improving the SNR for bicarbonate can have benefits for other human studies. Bicarbonate is a biomarker of PDH activity and plays a crucial role in the TCA cycle and tumor detection. However, the low concentration of bicarbonate limits the measurement in the human studies. In our study, we have proven the 3D MS-bSSFP bicarbonate sequence can work well on the brain (Figure 4) and kidney (Figure 5) in vivo.

Considering the bSSFP sequence is a T_1/T_2 weighted technique, the dynamic HP ^{13}C signal of the MS-bSSFP sequence is decreased due to both T_1 relaxation and T_2 relaxation.[43] It indicates that MS-bSSFP sequence has the potential to fit both T_1 and T_2 in vivo. In the current study, we did not consider the effect of blood flow, which can lead to a dynamic elongation of T_1 and T_2 in the organs.[44,56] However, comparing the signal ratio of 3D MS-bSSFP and 2D MS-GRE between animal data and simulation results (Figure 3), the animal data matches well when $T_2 = 0.5$ s for bicarbonate and $T_2 = 1.1$ s for lactate,

which matches well to results in previous literature[57] and indicates the T_2 of lactate and bicarbonate is relatively stable in the first 45 s of acquisition time in the healthy kidneys of Sprague-Dawley rats.

In the simulation of Figure S2(b), the optimal flip angle is affected by T_2 relaxation time. To match the effective flip angle in GRE sequence, the flip angle of MS-bSSFP sequence was set as 60°. The animal studies using this flip angle demonstrated an improvement in SNR of approximately 2.6±0.5× to 3±0.9×. In future studies, it would be useful to optimize the flip angle of 3D MS-bSSFP sequence to further improve the SNR of bicarbonate data.

Another open challenge with MS-bSSFP is quantification. In particular, current kinetic modeling methods[58] only incorporate GRE signal models and do not account for refocusing or T_2 relaxation that affect the bSSFP signal. Therefore, the T_2 mapping is likely to be useful for both flip angle optimization and kinetic modeling of 3D MS-bSSFP sequence. When combining MS-GRE and MS-bSSFP data, they will also experience different point spread functions and SNR efficiency. These are both a result of the differences in readout duration, where MS-GRE typically uses longer readouts that suffer more T2* and off-resonance blurring, as well as potential blurring across the multiple encoding steps required in MS-bSSFP (see above), and must be considered when developing analysis methods combining MS-GRE and MS-bSSFP data.

5. Conclusion

In conclusion, we have developed an efficient approach for imaging ^{13}C-bicarbonate in HP [1-^{13}C]pyruvate in vivo studies. Due to the repeated usage of the transverse magnetization, the 3D MS-bSSFP method with bicarbonate-specific RF pulses and optimized TR provided approximately 2–3× improved SNR than a GRE acquisition. With the advantage of short readout durations compared with GRE methods, this MS-bSSFP method can also reduce blurring artifacts caused by spiral trajectory. By combining ^{13}C-bicarbonate and [1-^{13}C]lactate 3D MS-bSSFP, we achieved improved SNR of both metabolites, without affecting ^{13}C pyruvate imaging. This advancement enables better observation of this low concentration metabolite, providing a potential way to investigate TCA cycle flux and pyruvate oxidation.

Supplementary Material

Refer to Web version on PubMed Central for supplementary material.

Acknowledgement

We would like to acknowledge funding support from NIH grants P41EB013598, R21DK130002, R01CA249909, R33HL161816 an American Cancer Society Research Scholar Grant 131715-RSG-18–005-01-CCE. We thank Heather Daniel, Kimberly Okamoto, Mary Frost, Andrew Riselli, Romelyn Delos Santos and Evelyn Escobar for assistance with the human study.

References

1. Hanahan D, Weinberg RA. Hallmarks of cancer: The next generation. Cell. 2011;144(5):646–674. doi:10.1016/j.cell.2011.02.013 [PubMed: 21376230]

2. Hanahan D, Weinberg RA. The Hallmarks of Cancer Review Evolve Progressively from Normalcy via a Series of Pre. Vol 100.; 2000.
3. Welch DR, Hurst DR. Defining the Hallmarks of Metastasis. Cancer Res. 2019;79(12):3011–3027. doi:10.1158/0008-5472.CAN-19-0458 [PubMed: 31053634]
4. Ardenkjaer-Larsen JH, rn Fridlund B, Gram A, et al. Increase in Signal-to-Noise Ratio of >10,000 Times in Liquid-State NMR. Vol 2.; 2003. www.pnas.orgcgidoi10.1073pnas.1733835100
5. Tang S, Meng MV., Slater JB, et al. Metabolic imaging with hyperpolarized 13C pyruvate magnetic resonance imaging in patients with renal tumors—Initial experience. Cancer. 2021;127(15):2693–2704. doi:10.1002/cncr.33554 [PubMed: 33844280]
6. Nelson SJ, Kurhanewicz J, Vigneron DB, et al. Metabolic imaging of patients with prostate cancer using hyperpolarized [1–13C]pyruvate. Sci Transl Med. 2013;5(198). doi:10.1126/scitranslmed.3006070
7. Lee PM, Chen H, Gordon JW, et al. Whole-Abdomen Metabolic Imaging of Healthy Volunteers Using Hyperpolarized [1-13C]pyruvate MRI. Journal of Magnetic Resonance Imaging. Published online April 14, 2022. doi:10.1002/jmri.28196
8. Wang ZJ, Ohliger MA, Larson PEZ, et al. Hyperpolarized 13C MRI: State of the art and future directions. Radiology. 2019;291(2):273–284. doi:10.1148/radiol.2019182391 [PubMed: 30835184]
9. Cunningham CH, Lau JYC, Chen AP, et al. Hyperpolarized 13C Metabolic MRI of the Human Heart: Initial Experience. Circ Res. 2016;119(11):1177–1182. doi:10.1161/CIRCRESAHA.116.309769 [PubMed: 27635086]
10. McLean M, Daniels C, Grist J, et al. Feasibility of metabolic imaging of hyperpolarized 13C-pyruvate in human breast cancer. . Magnetic Resonance Materials in Physics, Biology, and Medicine. Published online 2018.
11. Miloushev VZ, Granlund KL, Boltyanskiy R, et al. Metabolic imaging of the human brain with hyperpolarized 13C Pyruvate demonstrates 13C lactate production in brain tumor patients. Cancer Res. 2018;78(14):3755–3760. doi:10.1158/0008-5472.CAN-18-0221 [PubMed: 29769199]
12. Warburg O SCIENCE Injuring of Respiration On the Origin of Cancer Cells. Vol 123.; 1956. http://science.sciencemag.org/
13. Golman K, Zandt RI t., Lerche M, Pehrson R, Ardenkjaer-Larsen JH. Metabolic imaging by hyperpolarized 13C magnetic resonance imaging for in vivo tumor diagnosis. Cancer Res. 2006;66(22):10855–10860. doi:10.1158/0008-5472.CAN-06-2564 [PubMed: 17108122]
14. Spielman DM, Mayer D, Yen YF, Tropp J, Hurd RE, Pfefferbaum A. In vivo measurement of ethanol metabolism in the rat liver using magnetic resonance spectroscopy of hyperpolarized [1–13C]pyruvate. Magn Reson Med. 2009;62(2):307–313. doi:10.1002/mrm.21998 [PubMed: 19526498]
15. Schroeder MA, Cochlin LE, Heather LC, Clarke K, Radda GK, Tyler DJ. In Vivo Assessment of Pyruvate Dehydrogenase Flux in the Heart Using Hyperpolarized Carbon-13 Magnetic Resonance; 2008. www.pnas.orgcgidoi10.1073pnas.0805953105
16. Marquis Norman R, Fritz Irving B The Distribution of Carnitine, Acetylcarnitine, and Carnitine Acetyltransferase in Rat Tissues*.; 1964. doi:10.1016/S0021-9258(18)97445-4
17. Dienel GA. Brain Glucose Metabolism: Integration of Energetics with Function. Physiol Rev. 2019;99:949–1045. doi:10.1152/phys [PubMed: 30565508]
18. Larson PEZ, Chen HY, Gordon JW, et al. Investigation of analysis methods for hyperpolarized 13C-pyruvate metabolic MRI in prostate cancer patients. NMR Biomed. 2018;31(11). doi:10.1002/nbm.3997
19. Park JM, Reed GD, Liticker J, et al. Effect of Doxorubicin on Myocardial Bicarbonate Production from Pyruvate Dehydrogenase in Women with Breast Cancer. Circ Res. 2020;127(12):1568–1570. doi:10.1161/CIRCRESAHA.120.317970 [PubMed: 33054563]
20. Li Y, Vigneron DB, Xu D. Current human brain applications and challenges of dynamic hyperpolarized carbon-13 labeled pyruvate MR metabolic imaging. Eur J Nucl Med Mol Imaging. 2021;48(13):4225–4235. doi:10.1007/s00259-021-05508-8 [PubMed: 34432118]
21. Rider OJ, Apps A, Miller JJJJ, et al. Noninvasive in vivo assessment of cardiac metabolism in the healthy and diabetic human heart using hyperpolarized 13C MRI. Circ Res. Published online 2020:725–736. doi:10.1161/CIRCRESAHA.119.316260 [PubMed: 32078413]

22. Park JM, Spielman DM, Josan S, et al. Hyperpolarized 13C-lactate to 13C-bicarbonate ratio as a biomarker for monitoring the acute response of anti-vascular endothelial growth factor (anti-VEGF) treatment. NMR Biomed. 2016;29(5):650–659. doi:10.1002/nbm.3509 [PubMed: 26990457]

23. Merritt ME, Harrison C, Sherry AD, Malloy CR, Burgess SC. Flux through hepatic pyruvate carboxylase and phosphoenolpyruvate carboxykinase detected by hyperpolarized 13C magnetic resonance. Proc Natl Acad Sci U S A. 2011;108(47):19084–19089. doi:10.1073/pnas.1111247108 [PubMed: 22065779]

24. Nielsen PM, Qi H, Bertelsen LB, Laustsen C. Metabolic reprogramming associated with progression of renal ischemia reperfusion injury assessed with hyperpolarized [1–13C]pyruvate. Sci Rep. 2020;10(1). doi:10.1038/s41598-020-65816-1

25. Li Y, Vigneron DB, Xu D. Current human brain applications and challenges of dynamic hyperpolarized carbon-13 labeled pyruvate MR metabolic imaging. Eur J Nucl Med Mol Imaging. 2021;48(13):4225–4235. doi:10.1007/s00259-021-05508-8 [PubMed: 34432118]

26. Roemer PB, Edelstein WA, Hayes CE, Souza SP, Mueller M. The NMR Phased Array. Vol 16.; 1990.

27. Gordon JW, Vigneron DB, Larson PEZ. Development of a symmetric echo planar imaging framework for clinical translation of rapid dynamic hyperpolarized 13C imaging. Magn Reson Med. 2017;77(2):826–832. doi:10.1002/mrm.26123 [PubMed: 26898849]

28. Milshteyn E, von Morze C, Gordon JW, Zhu Z, Larson PEZ, Vigneron DB. High spatiotemporal resolution bSSFP imaging of hyperpolarized [1–13C]pyruvate and [1–13C]lactate with spectral suppression of alanine and pyruvate-hydrate. Magn Reson Med. 2018;80(3):1048–1060. doi:10.1002/mrm.27104 [PubMed: 29451329]

29. Tang S, Bok R, Qin H, et al. A metabolite-specific 3D stack-of-spiral bSSFP sequence for improved lactate imaging in hyperpolarized [1–13C]pyruvate studies on a 3T clinical scanner. Magn Reson Med. 2020;84(3):1113–1125. doi:10.1002/mrm.28204 [PubMed: 32086845]

30. Gordon JW, Autry AW, Tang S, et al. A variable resolution approach for improved acquisition of hyperpolarized 13C metabolic MRI. Magn Reson Med. 2020;84(6):2943–2952. doi:10.1002/mrm.28421 [PubMed: 32697867]

31. Maidens J, Gordon JW, Arcak M, Larson PEZ. Optimizing Flip Angles for Metabolic Rate Estimation in Hyperpolarized Carbon-13 MRI. IEEE Trans Med Imaging. 2016;35(11):2403–2412. doi:10.1109/TMI.2016.2574240 [PubMed: 27249825]

32. Korenchan DE, Gordon JW, Subramaniam S, et al. Using bidirectional chemical exchange for improved hyperpolarized [13C]bicarbonate pH imaging. Magn Reson Med. 2019;82(3):959–972. doi:10.1002/mrm.27780 [PubMed: 31050049]

33. Somai V, Wright AJ, Fala M, Hesse F, Brindle KM. A multi spin echo pulse sequence with optimized excitation pulses and a 3D cone readout for hyperpolarized 13C imaging. Magn Reson Med. 2020;84(4):1895–1908. doi:10.1002/mrm.28248 [PubMed: 32173908]

34. Josan S, Yen YF, Hurd R, Pfefferbaum A, Spielman D, Mayer D. Application of double spin echo spiral chemical shift imaging to rapid metabolic mapping of hyperpolarized [1 – 13C]-pyruvate. Journal of Magnetic Resonance. 2011;209(2):332–336. doi:10.1016/j.jmr.2011.01.010 [PubMed: 21316280]

35. Cunningham CH, Chen AP, Albers MJ, et al. Double spin-echo sequence for rapid spectroscopic imaging of hyperpolarized 13C. Journal of Magnetic Resonance. 2007;187(2):357–362. doi:10.1016/j.jmr.2007.05.014 [PubMed: 17562376]

36. Yen YF, Roux P Le, Mayer D, et al. T2 relaxation times of 13C metabolites in a rat hepatocellular carcinoma model measured in vivo using 13C-MRS of hyperpolarized [1–13C]pyruvate. NMR Biomed. 2010;23(4):414–423. doi:10.1002/nbm.1481 [PubMed: 20175135]

37. Leupold J, Månsson S, Stefan Petersson J, Hennig J, Wieben O. Fast multiecho balanced SSFP metabolite mapping of 1H and hyperpolarized 13C compounds. Magnetic Resonance Materials in Physics, Biology and Medicine. 2009;22(4):251–256. doi:10.1007/s10334-009-0169-z

38. Liu X, Tang S, Mu C, et al. Development of specialized magnetic resonance acquisition techniques for human hyperpolarized [13C,15N2]urea + [1-13C]pyruvate simultaneous perfusion and metabolic imaging. Magn Reson Med. Published online May 8, 2022. doi:10.1002/mrm.29266

39. Kettunen MI, Hu DE, Witney TH, et al. Magnetization transfer Measurements of exchange between hyperpolarized [1–13C]pyruvate and [1–13C]lactate in a murine lymphoma. Magn Reson Med. 2010;63(4):872–880. doi:10.1002/mrm.22276 [PubMed: 20373388]
40. Shang H, Larson PEZ, Kerr A, et al. Multiband RF pulses with improved performance via convex optimization. Journal of Magnetic Resonance. 2016;262:81–90. doi:10.1016/j.jmr.2015.11.010 [PubMed: 26754063]
41. Larson PEZ, Kerr AB, Chen AP, et al. Multiband excitation pulses for hyperpolarized 13C dynamic chemical-shift imaging. Journal of Magnetic Resonance. 2008;194(1):121–127. doi:10.1016/j.jmr.2008.06.010 [PubMed: 18619875]
42. Sahin SI, Ji X, Agarwal S, et al. Metabolite-Specific Echo Planar Imaging for Preclinical Studies with Hyperpolarized 13C-Pyruvate MRI. Tomography. 2023;9(2):736–749. doi:10.3390/tomography9020059 [PubMed: 37104130]
43. Svensson J, Månsson S, Johansson E, Petersson JS, Olsson LE. Hyperpolarized 13C MR angiography using trueFISP. Magn Reson Med. 2003;50(2):256–262. doi:10.1002/mrm.10530 [PubMed: 12876701]
44. Reed GD, von Morze C, Verkman AS, et al. Imaging Renal Urea Handling in Rats at Millimeter Resolution Using Hyperpolarized Magnetic Resonance Relaxometry. Tomography. 2016;2(2):125–137. doi:10.18383/j.tom.2016.00127 [PubMed: 27570835]
45. Ma J, Chen J, Reed GD, et al. Cardiac T2* measurement of hyperpolarized 13C metabolites using metabolite-selective multi-echo spiral imaging. Magn Reson Med. 2021;86(3):1494–1504. doi:10.1002/mrm.28796 [PubMed: 33821504]
46. Hyperpolarized-MRI-Toolbox. https://github.com/LarsonLab/hyperpolarized-mri-toolbox.
47. Tang S, Jiang W, Chen HY, Bok R, Vigneron DB, Larson PEZ. A 2DRF pulse sequence for bolus tracking in hyperpolarized 13C imaging. Magn Reson Med. 2015;74(2):506–512. doi:10.1002/mrm.25427 [PubMed: 25154961]
48. Tang S, Milshteyn E, Reed G, et al. A regional bolus tracking and real-time B1 calibration method for hyperpolarized 13C MRI. Magn Reson Med. 2019;81(2):839–851. doi:10.1002/mrm.27391 [PubMed: 30277268]
49. Jackson JI, Meyer CH, Nishimura DG, Macovski A. Selection of a Convolution Function for Fourier Inversion Using Gridding. IEEE Trans Med Imaging. 1991;10(3):473–478. doi:10.1109/42.97598 [PubMed: 18222850]
50. Pruessmann KP, Weiger M, Bö P, Boesiger P. Advances in Sensitivity Encoding With Arbitrary K-Space Trajectories.; 2001.
51. Zhu Z, Zhu X, Ohliger MA, et al. Coil combination methods for multi-channel hyperpolarized 13 C imaging data from human studies. Journal of Magnetic Resonance. 2019;301:73–79. doi:10.1016/j.jmr.2019.01.015 [PubMed: 30851668]
52. Miller AJ, Joseph PM. THE USE OF POWER IMAGES TO PERFORM QUANTITATIVE ANALYSIS ON LOW SNR MR IMAGES.; 1993.
53. Varma G, Wang X, Vinogradov E, et al. Selective spectroscopic imaging of hyperpolarized pyruvate and its metabolites using a single-echo variable phase advance method in balanced SSFP. Magn Reson Med. 2016;76(4):1102–1115. doi:10.1002/mrm.26004 [PubMed: 26507361]
54. Lee CY, Soliman H, Geraghty BJ, et al. Lactate topography of the human brain using hyperpolarized 13C-MRI. Neuroimage. 2020;204. doi:10.1016/j.neuroimage.2019.116202
55. Grist JT, McLean MA, Riemer F, et al. Quantifying normal human brain metabolism using hyperpolarized [1– 13 C]pyruvate and magnetic resonance imaging. Neuroimage. 2019;189:171–179. doi:10.1016/j.neuroimage.2019.01.027 [PubMed: 30639333]
56. Reed GD, von Morze C, Bok R, et al. High resolution 13C MRI with hyperpolarized urea: In vivo T 2 mapping and 15N labeling effects. IEEE Trans Med Imaging. 2014;33(2):362–371. doi:10.1109/TMI.2013.2285120 [PubMed: 24235273]
57. Grashei M, Hundshammer C, van Heijster FHA, Topping GJ, Schilling F. PH dependence of T2 for hyperpolarizable 13C-labelled small molecules enables spatially resolved pH measurement by magnetic resonance imaging. Pharmaceuticals. 2021;14(4). doi:10.3390/ph14040327

58. Mammoli D, Carvajal L, Slater JB, et al. Kinetic Modeling of Hyperpolarized Carbon-13 Pyruvate Metabolism in the Human Brain. IEEE Trans Med Imaging. 2020;39(2):320–327. doi:10.1109/TMI.2019.2926437 [PubMed: 31283497]

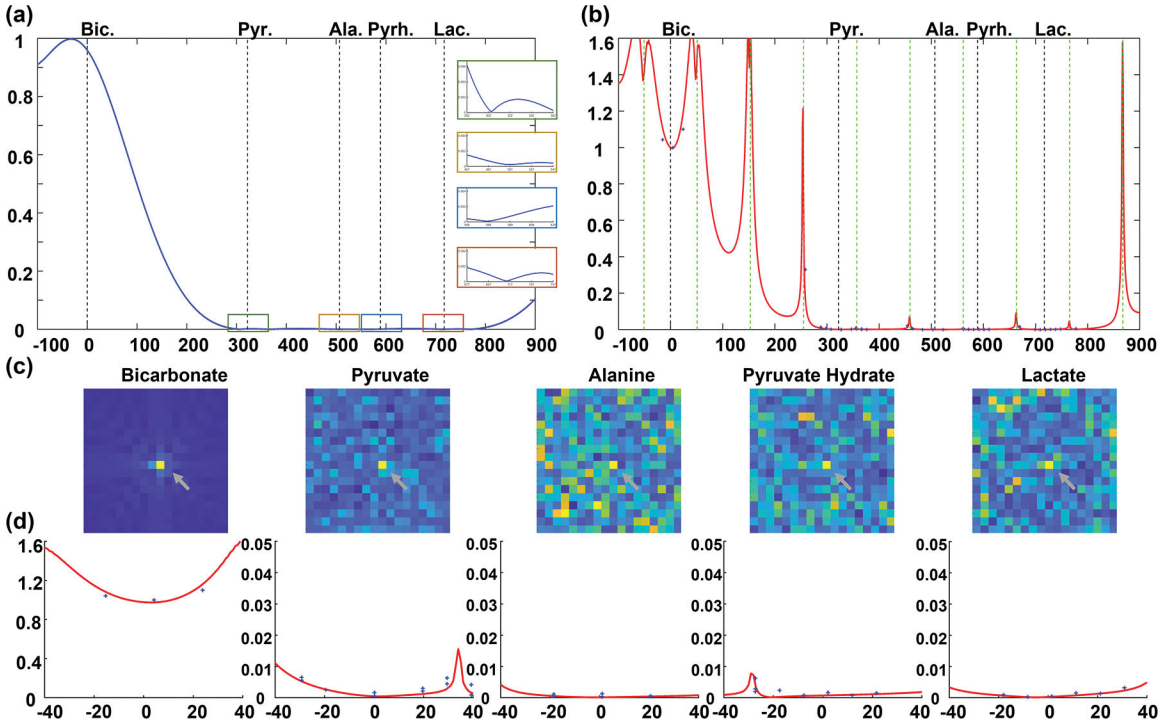

FIGURE 1.

(a&b) The excitation profiles of MS-bSSFP bicarbonate sequence simulated by Bloch equation. (a) The excitation profile of bicarbonate-specific RF pulse alone with zoomed views (±40 Hz) at each metabolite frequency on the right side. (b) The excitation profile of the RF pulse in a MS-bSSFP sequence (magnetization from the mean of 64 RF pulses). The banding artifacts were shown by vertical green dot lines. (c) ^{13}C urea phantom results (shown by grey arrays) acquired by bicarbonate MS-bSSFP sequence. (d) The excitation profiles in zoomed view (±40 Hz) at each metabolite frequency. The blue cross points indicate the normalized signals of urea phantom.

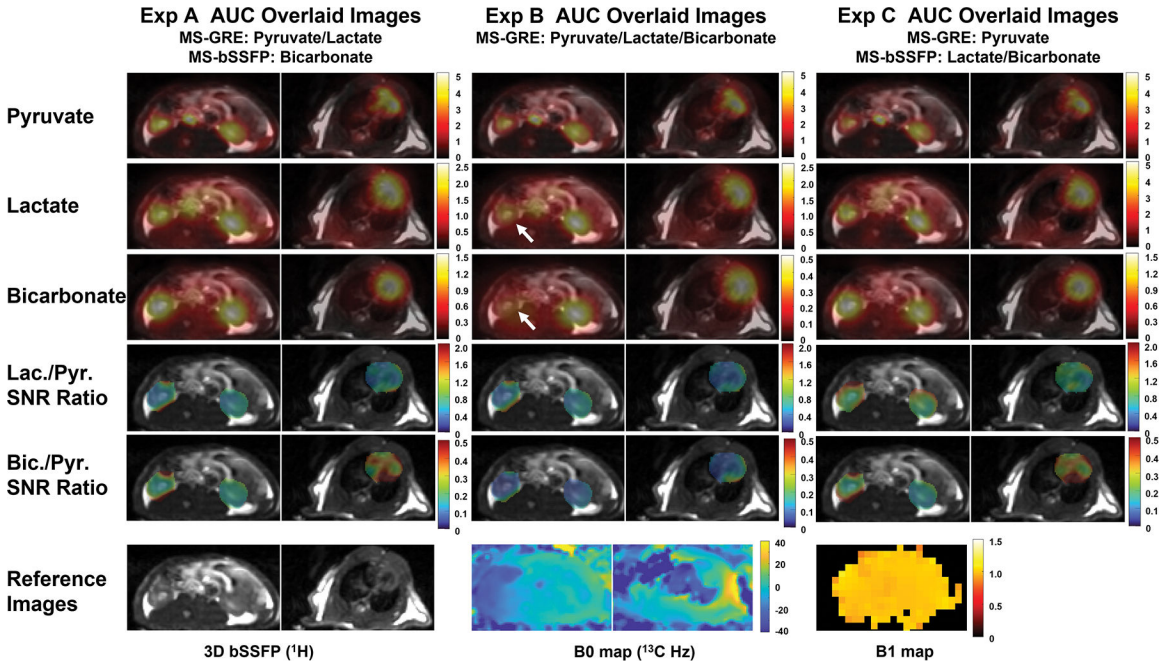

FIGURE 2.

Comparison between 3D MS-bSSFP sequence and 2D MS-GRE sequence in a healthy rat, using three different experiments: pyruvate and lactate 2D MS-GRE, bicarbonate 3D MS-bSSFP in Experiment A; pyruvate, lactate and bicarbonate 2D MS-GRE in Experiment B; pyruvate 2D MS-GRE, lactate and bicarbonate 3D MS-bSSFP in Experiment C. AUC images are scaled by maximum signal of each metabolite, while lactate-to-pyruvate and bicarbonate-to-pyruvate SNR ratio images are presented by a fixed scale range. The right kidney shows more blurring artifact with the lactate and bicarbonate 2D MS-GRE sequences compared to the 3D MS-bSSFP sequence (shown by grey arrows). This can be ascribed to the larger off-resonance frequency.

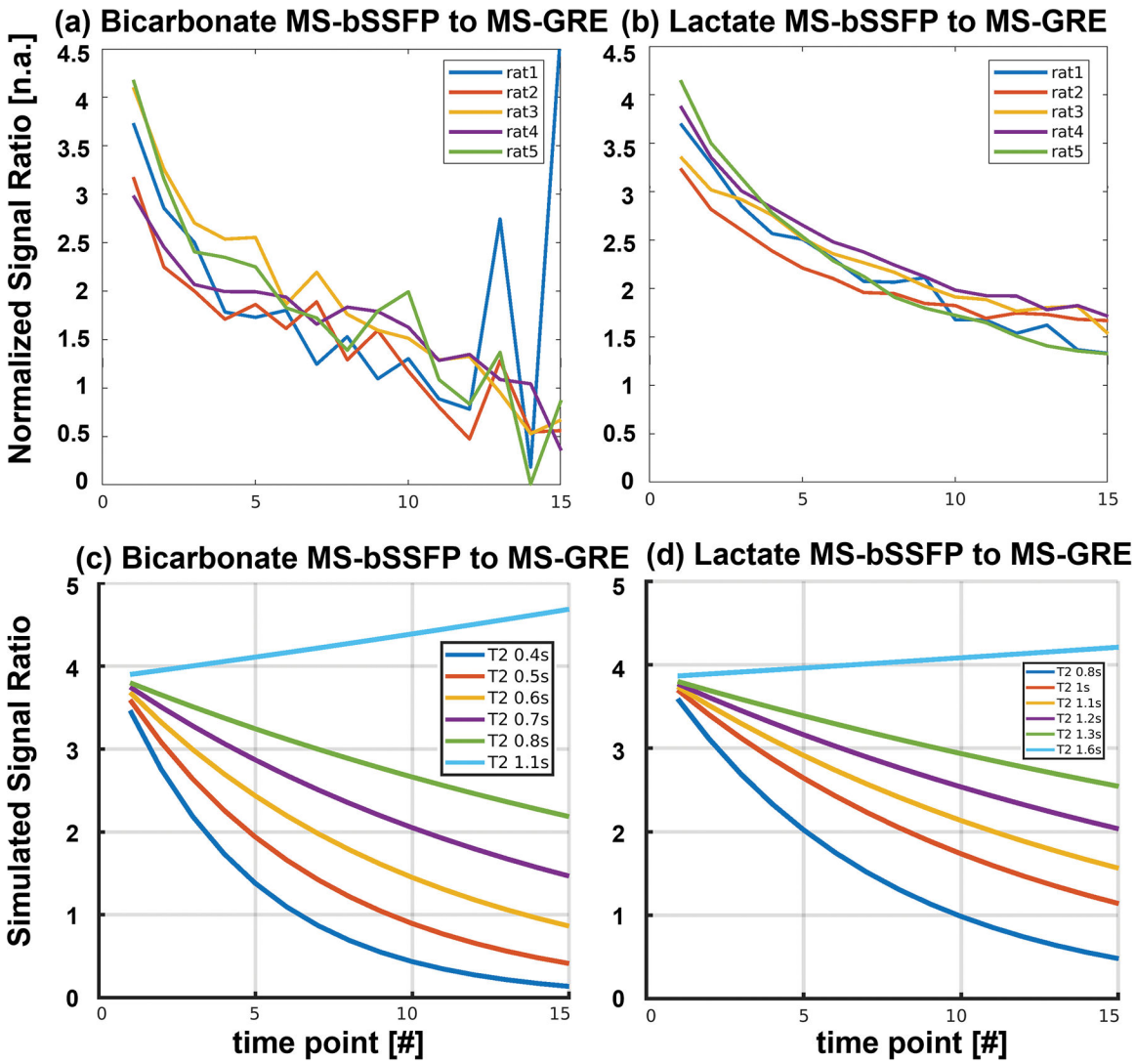

FIGURE 3.

3D bicarbonate MS-bSSFP to 2D bicarbonate MS-GRE SNR ratio and 3D lactate MS-bSSFP to 2D lactate MS-GRE SNR ratio of five healthy Sprague Dawley rat kidneys (a&b) and corresponding simulations (c&d). The signals were measured on the kidneys of each rat with a voxel SNR threshold higher than 3.

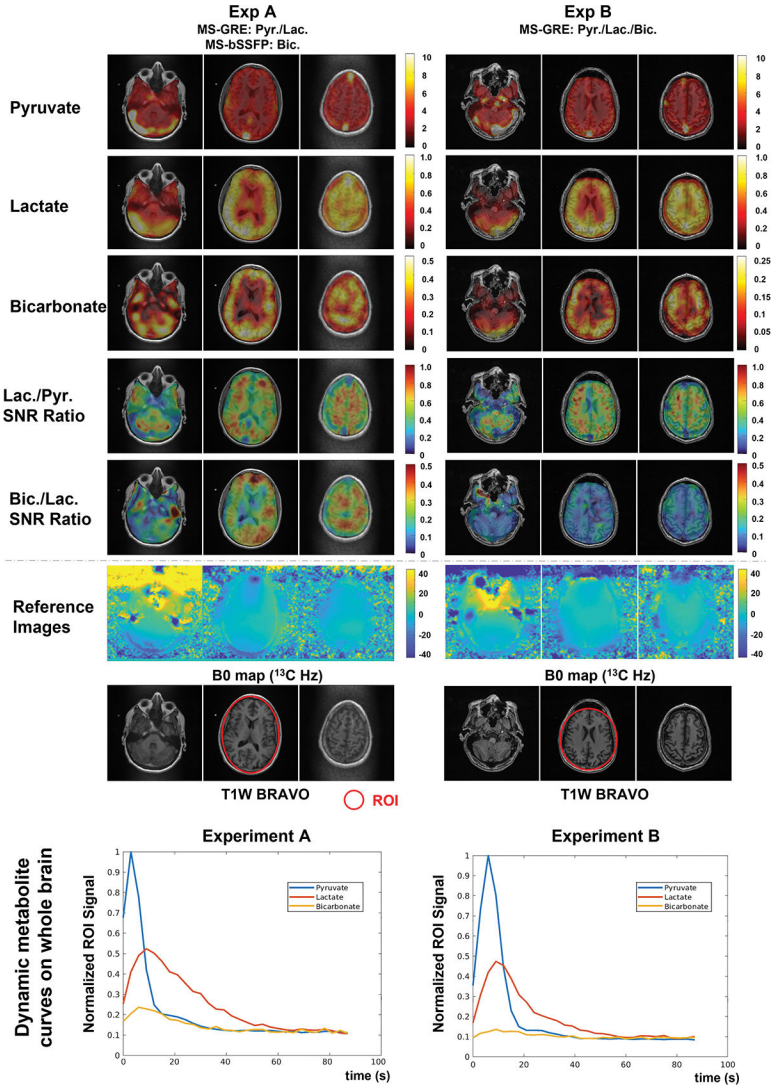

FIGURE 4.

AUC images of pyruvate, lactate, and bicarbonate, and bicarbonate-to-lactate SNR ratio maps and dynamic whole brain ROI curves of pyruvate, lactate, and bicarbonate on the brain of two volunteers. AUC images are scaled by the maximum signal of each metabolite, while bicarbonate-to-lactate and lactate-to-pyruvate SNR ratio images are presented by the fixed scale range, showing a higher bicarbonate SNR acquired by the 3D MS-bSSFP sequence than the 2D MS-GRE sequence. The SNR of the bicarbonate signal on both volunteers peaks at around 8 s after acquisition starts. The normalized bicarbonate SNR peak of 3D MS-bSSFP is approximately 2.1 times higher than the normalized SNR peak of 2D MS-GRE across the brain.

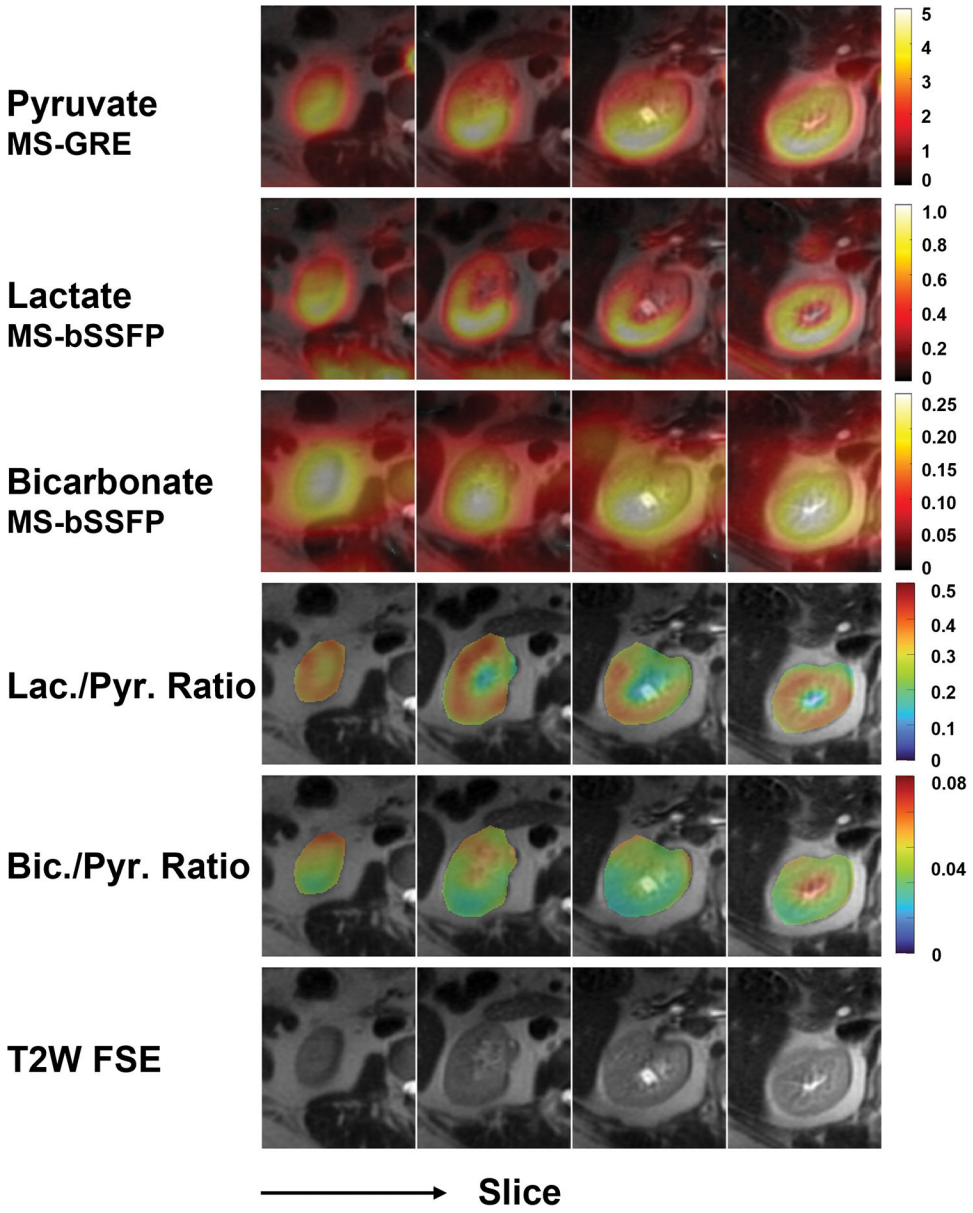

FIGURE 5.

Hyperpolarized ^{13}C AUC images of pyruvate, lactate, and bicarbonate of a human kidney. The lactate-to-pyruvate and bicarbonate-to-pyruvate SNR ratio maps are displayed using a fixed scale range.

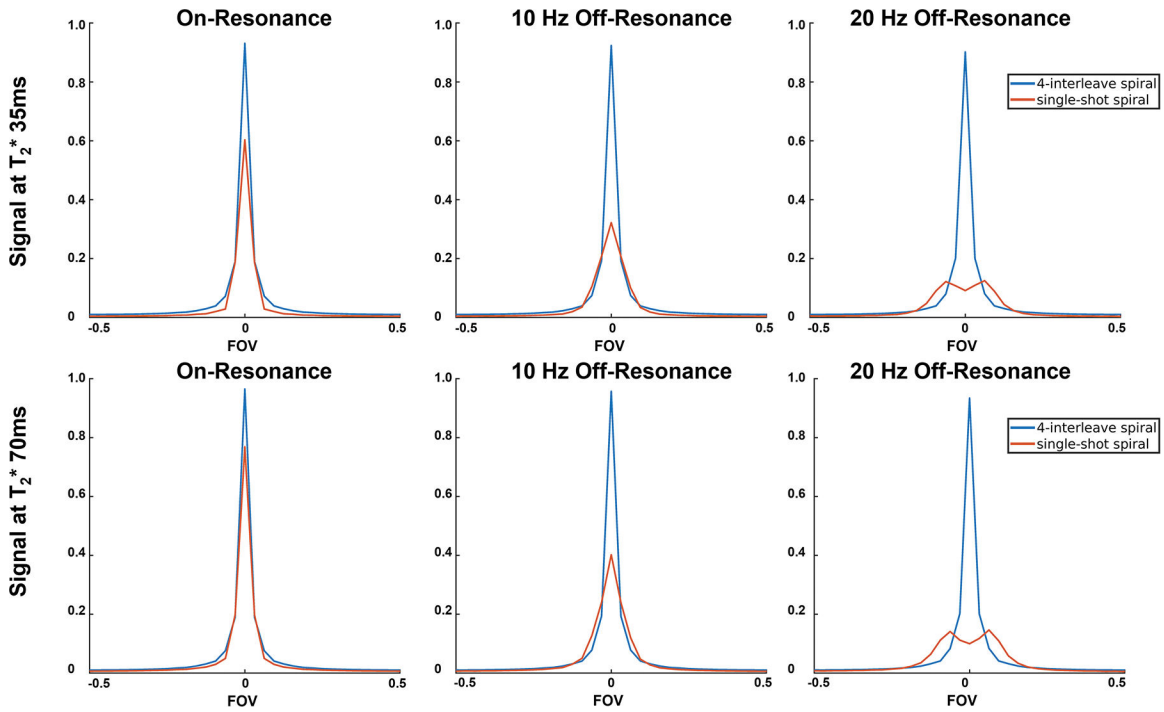

FIGURE 6.

Point spread functions of the 4-interleave spiral readout used in the MS-bSSFP sequence and the single-shot spiral readout used in the MS-GRE sequence with 0/10/20 Hz off-resonance frequencies and 35/70ms T_2* relaxation times.

TABLE 1

Summary of acquisition parameters in HP [1-^{13}C]pyruvate imaging animal studies and human studies. Note that while the voxel dimensions changed between Experiment A and B for the human studies, the voxel volumes were fixed so we could compare SNR across experiments.

(a) Acquisition parameters in animal Study			
	Experiment A	**Experiment B**	**Experiment C**
Pyruvate	2D MS-GRE FOV 8×8×16.8 cm^3, resolution 2.5×2.5×21 mm^3, TR 100 ms		
Lactate	2D MS-GRE resolution 5×5×21 mm^3, TR 100 ms		3D MS-bSSFP resolution 5×5×21 mm^3
Bicarbonate	3D MS-bSSFP resolution 7.5×7.5×21 mm^3	2D MS-GRE resolution 7.5×7.5×21 mm^3, TR 100 ms	3D MS-bSSFP resolution 7.5×7.5×21 mm^3
ALL	Temporal resolution 2.5 s, 30 timepoints		Temporal resolution 2.8 s, 30 timepoints

(b) Acquisition parameters in human brain study		
	Experiment/Subject A	**Experiment/Subject B**
Pyruvate	2D MS-GRE FOV 24×24×15 cm^3, resolution 7.5×7.5×15 mm^3 (**0.84 cc**), TR 110 ms	2D MS-GRE FOV 31.7×31.7×16.8 cm^3, resolution 6.34×6.34×21 mm^3 (**0.84 cc**), TR 125 ms
Lactate	2D MS-GRE resolution 15×15×15 mm^3 (**3.37 cc**), TR 110 ms	2D MS-GRE resolution 12.68×12.68×21 mm^3 (**3.37 cc**), TR 125 ms,
Bicarbonate	3D MS-bSSFP FOV 24×24×24 cm^3, resolution 15×15×15 mm^3(**3.37 cc**)	2D MS-GRE FOV 31.7×31.7×16.8 cm^3, resolution 12.68×12.68×21 mm^3(**3.37 cc**), TR 125 ms
ALL	temporal resolution 3 s, 30 timepoints	
B_1^+ Mapping	2D MS-GRE with Bloch Siegert method on pyruvate frequency FOV 45×45×9 cm^3, resolution 1.5×1.5×30 mm^3, slice gap = 4.5 cm, 3 slices, TR 200 ms, flip angle 8°, ω_{RF} 4.5 kHz	

(c) Acquisition parameters in human renal study	
Pyruvate	2D MS-GRE FOV 50×50 cm^2, resolution 1×1×2.1 cm^3, TR 80 ms
Lactate	3D MS-bSSFP FOV 46×46×33.6 cm^3, resolution 1×1×2.1 cm^3
Bicarbonate	3D MS-bSSFP FOV 92×92×33.6 cm^3, resolution 2×2×2.1 cm^3
ALL	temporal resolution 3.5 s, 30 timepoints

(d) Common Sequence Parameters	
2D MS-GRE	T_{read} 22 ms, flip angle 20° (pyruvate) or 30° (lactate and bicarbonate), 8 slices
3D MS-bSSFP	T_{read} 3.8 ms, flip angle 60°, echo train length 64, TR 9.8 ms (bicarbonate) or 15.29 ms (lactate), 16 slices

Notes: (a) Three experiments (A, B&C) were conducted to compare the lactate and bicarbonate signal acquired by two different sequences. In experiment A, 2D MS-GRE sequence was used to acquire pyruvate and lactate signals and 3D MS-bSSFP sequence was used to acquire bicarbonate signal. In experiment B, 2D MS-GRE sequence was used to acquire all metabolite signals. In experiment C, 2D MS-GRE sequence was used to acquire pyruvate signal and 3D MS-bSSFP sequences were used to acquire lactate and bicarbonate signals; (b) Two experiments (A and B) were conducted to compare the bicarbonate signal in the human brain using 2D MS-GRE and 3D MS-bSSFP sequences, respectively; (c) A clinical trial was conducted on a patient with RCC to demonstrate the feasibility of the MS-bSSFP sequence.